




Promoter methylation in a mixed feedback loop circadian clock model

Turner Silverthorne ^{1,2}, Edward Saehong Oh ², and Adam R. Stinchcombe ^{1,*}

¹*Department of Mathematics, University of Toronto, Toronto, M5S 2E4 Ontario, Canada*

²*The Krembil Family Epigenetics Laboratory, The Campbell Family Mental Health Research Institute, Centre for Addiction and Mental Health, Toronto, M5T 1R8 Ontario, Canada*



(Received 1 September 2021; revised 24 February 2022; accepted 27 February 2022; published 30 March 2022)

We investigate how epigenetic modifications to clock gene promoters affect transcriptomic activity in the circadian clock. Motivated by experimental observations that link DNA methylation with the behavior of the clock, we introduce and analyze an extension of the mixed feedback loop (MFL) model of François and Hakim. We extend the original model to include an additional methylated promoter state and allow for reversible protein sequestration, an important feature for circadian applications. First, working with the general form of the MFL model, we find that the qualitative behavior of the model is dictated by the promoter state with the highest transcription rate. We then build on the work of Kim and Forger, who analyzed the stability of the mammalian circadian clock by using a reduced form of the MFL model. We present a rigorous procedure for translating between the MFL model and the reduction of Kim and Forger. We then propose a model reduction more appropriate for the study of oscillatory promoter states, making use of a fully coupled quasi-steady-state approximation rather than the standard partially uncoupled quasi-steady-state approach. Working with the novel reduced form of the model, we find substantial differences in the transcription function and show that, although methylation contributes to period control, excessive methylation can abolish rhythmicity. Altogether our results show that even in a minimal clock model, DNA methylation has a nontrivial influence on the system's ability to oscillate.

DOI: [10.1103/PhysRevE.105.034411](https://doi.org/10.1103/PhysRevE.105.034411)

I. INTRODUCTION

Epigenetic DNA modifications are far more dynamic than their traditional depiction [1,2]. Indeed, the modification status of cytosines (5-mC, 5-hmC, 5-fC, and 5-caC) can vary significantly with various timescales: years or age [3], hours [4–6], and minutes [7,8]. Ongoing experimental efforts have focused on the relevance of epigenetic oscillations to biological function and phenotypes. In this paper, we focus on a particular instance of this general phenomenon: the influence of DNA methylation on the circadian clock.

Both steady-state and oscillatory differences in the methylation status of clock genes in mammals have been detected in recent years. Azzi *et al.* entrained mice to a 22 hour day and found that after removing the entrainment cue the mice retained a shortened circadian period and had differentially methylated clock genes [9]. Azzi *et al.* also found that the transcriptomic consequences of promoter methylation were gene-dependent. For example, the expression of the clock genes *Per2* and *Cry1* was inhibited by increased methylation, whereas the opposite was true of *Clock*. Interestingly, period changes were suppressed by chemically induced inhibition of methylation. From these observations, they hypothesized that DNA methylation of clock genes contributes to the plasticity of the mammalian circadian clock. More recently, circadian epigenomic studies have found evidence for 24-hour diurnal oscillations in cytosine modifications in

human neutrophils [5], as well as the mouse liver and lung [4]. Interestingly, a portion of stochastic intra and interindividual epigenetic variation was accounted for by oscillations [5], and sequences surrounding oscillating cytosine modifications were enriched in both canonical (CANNTG) and noncanonical (CANNNTG, GANNTG) enhancer elements [4] (known as E-boxes), which play key roles in regulation of circadian transcripts [10]. These features of oscillating cytosine modifications suggest that oscillations in cytosine modifications are intricately linked to circadian transcriptomics, possibly by regulating the epigenetic status of E-box motifs.

Our aim in this paper is to add a mathematical perspective to these intriguing experimental findings. To this end, we focus on the PER transcription-translation feedback loop (TTFL), which is known to be of primary importance for rhythm generation in the mammalian circadian clock. We model this system using an extension of the mixed feedback loop (MFL) model of François and Hakim [11]. The reader may be more familiar with the classic Goodwin model of the circadian clock [12]. We comment on similarities and differences between the MFL and Goodwin models in Sec. III D.

The MFL model was first presented as a simple gene regulatory network capable of a range of dynamic behaviours [13] such as multistability and nonlinear oscillations. The MFL model has been found to be present in a variety of biologically important networks. For instance, the circadian clocks of *Neurospora* [14] and *Drosophila* [13], the p53-Mdm2 module [15], and the *E. coli* lactose operon [16]. More recently, the MFL model was used in several studies as a minimal model of the circadian clock [17–20]. Building on the work of Kim and Forger [17], who used the MFL model in their analysis

*Corresponding author: stinch@math.toronto.edu

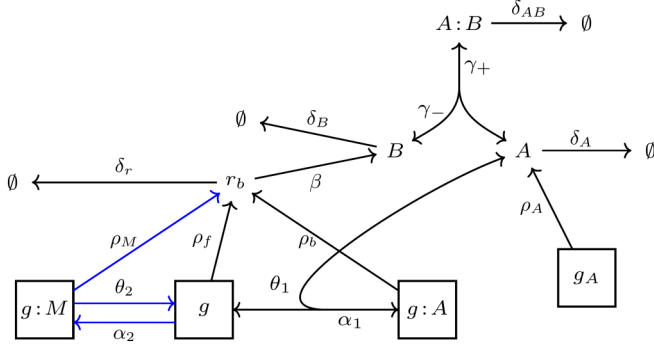


FIG. 1. Reaction diagram for the IT-MFL model. The activator A , with concentration $[A]$, is constitutively expressed, whereas the promoter of the target protein B , with concentration $[B]$, can be in an active, inactive, or methylated state with concentrations $[g : A]$, $[g]$, $[g : M]$, respectively. The concentration of the mRNA for protein B is $[r_b]$. Since B binds to A , which has concentration $[A : B]$, this sequestration mechanism forms a negative feedback loop. The parameters of the model are as follows: α_1 , the binding rate of A to g ; θ_1 , the unbinding rate of $g : A$; α_2 , the methylation rate of g ; θ_2 , the demethylation rate of $g : M$; ρ_M , the transcription rate of B for a methylated promoter; ρ_f , the transcription rate of B for an inactive promoter; ρ_b , the transcription rate of B for an active promoter; β , the translation rate of B ; ρ_A , the transcription rate of A ; γ_+ , the binding rate of A and B ; γ_- , the unbinding rate of $A : B$; δ_A , the degradation rate of A ; δ_B , the degradation rate of B ; δ_{AB} , the degradation rate of $A : B$; and δ_r , the degradation rate of r_b . Reactions present in the original MFL model are drawn in black and the reactions new to the IT-MFL model are drawn in blue.

of a detailed mammalian clock model, we add an additional promoter state to represent DNA methylation. Since the transcription rate of the new promoter state will be assumed to lie between the active and inactive transcription rates, we refer to our extension of the MFL model as the *intermediate transcription rate* MFL model (IT-MFL model). In some parts of our analysis, we also consider reversible protein binding which was crucial to the work of Kim and Forger, but was absent from the original papers on the MFL model.

Our analysis is divided into two parts. Inspired by the work of François and Hakim, we begin by studying the system perturbatively. We extend their boundary layer analysis to

derive approximate expressions for the period and bounds on the influence of methylation on the period in a limiting case of the model. A recurring theme in our perturbative analysis is that the MFL and IT-MFL models display qualitatively similar behavior at dominant order provided that the transcription rate of the new promoter state is, in fact, *intermediate*. In the second part, we extend the work of Kim and Forger [17]. In addition to simulating a detailed model of the clock, they also used a modified form of the Goodwin oscillator to test their hypothesis that a balanced stoichiometry between activators and repressors was necessary for autonomous oscillations in the clock. We show how their model [which takes the form of a three-dynamic-variable monotone cyclic feedback (MCF) system] can be obtained as an approximation of the IT-MFL model. We show that Kim and Forger's approximation of the MFL model can be obtained by decoupling the activator protein from the promoter states and making quasi-steady-state (QSS) approximations. We relax this assumption to allow for fully coupled quasi-steady-states and find that substantial differences emerge in the transcription function. Working in this novel approximation, our analysis reveals that, although the period and its derivatives in parameter space are sensitive to methylation, excessive methylation can abolish rhythmicity. For a wide range of promoter activation equilibrium constants, numerical bifurcation analysis reveals that this loss of rhythmicity occurs through a supercritical Hopf bifurcation. Additionally we find that methylation cannot be compensated for by varying the transcription rate of the inactive promoter state alone. The fact that the qualitative behavior of our model is sensitive to slight differences in transcriptional regulation aligns with the general principle that even slight changes in transcriptional regulation can dramatically alter the behavior of a genetic oscillator [21].

II. MATHEMATICAL MODEL

An illustration of the MFL model is given in Fig. 1, along with the extensions of the IT-MFL model. Our primary interest is in oscillatory solutions of the MFL and IT-MFL models, depicted in Figs. 2 and 3. The MFL model consists of an activator protein A which interacts with a target protein B . The activator is assumed to be constitutively expressed whereas B is regulated by a promoter that is active when bound to A

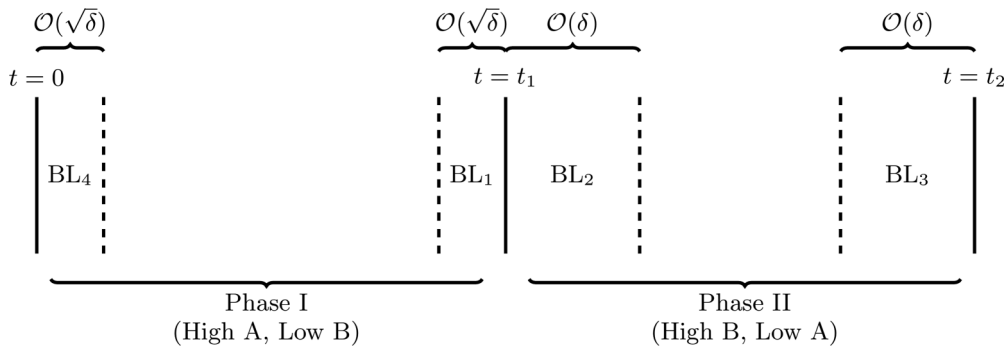


FIG. 2. Structure of the boundary layers in a limit-cycle solution to the MFL model. Boundary layers BL_2 and BL_3 form when the system transitions from a phase of high A to high B concentration. Boundary layers BL_1 and BL_4 appear as the quasi-steady-state approximation for g breaks down.

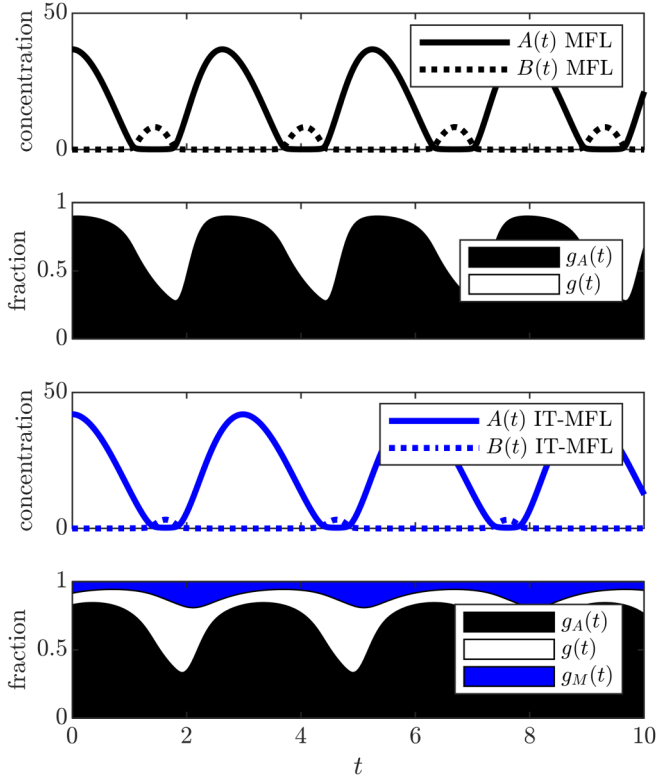


FIG. 3. Oscillatory solutions to the MFL and IT-MFL models. In both cases, the oscillatory solutions decompose into phases of high A –low B (Phase I) and high B –low A (Phase II) concentration. Promoter states are shown for both models. Simulation parameters: $\delta = 3 \times 10^{-3}$, $\rho_0 = 0$, $\rho_1 = 1.45$, $\tilde{\theta}_1 = 1.33$, $d_a = 0.33$, $d_b = 0.33$, $\mu = 0.31$, $A_0 = 4$, $\rho_2 = 0$, $\tilde{\alpha}_2 = 1$, $\tilde{\theta}_2 = 2$.

and otherwise inactive. Finally, B can bind to A , sequestering it away from its promoters and thereby repressing its own transcription [22,23]. The MFL model has been applied in several biological contexts, including the work of Kim and Forger on circadian rhythms [17]. When studied in the context of the mammalian circadian clock, the activator A and target protein B represent CLOCK-BMAL1 and PER, respectively. Although the clock is made up of several interlocking feedback loops, the PER TTFL is a well-established starting point for a minimal model for analyzing the dynamics of this complex system [17].

We extend the MFL model in two ways: we add a new promoter state to represent methylation of the PER E-boxes and allow for the unbinding of A and B . Some effects of the unbinding were discussed by Kim and Forger in a reduced form of the MFL model, but to the best of our knowledge this has not yet been studied in the full MFL model. As mentioned in the Introduction, we assume the transcription rate corresponding to the methylated promoter state lies between the transcription rates of the active and inactive states. Although DNA methylation and demethylation are catalyzed by a variety of enzymes, the IT-MFL model assumes these reactions are operating with first-order kinetics. Explicit incorporation of the methylation and demethylation enzymes would be a natural next step to this work. Our analysis in this section follows the methodology from the original paper of

François and Hakim and so we adopt their notation for our model.

Parameters, dynamic variables, and governing equations

We use mass-action kinetics [24] to obtain the following governing the promoter states:

$$\frac{d[g]}{dt} = \theta_1[g : A] + \theta_2[g : M] - \alpha_1[g][A] - \alpha_2[g], \quad (1)$$

$$\frac{d[g : M]}{dt} = \alpha_2[g] - \theta_2[g : M], \quad (2)$$

$$\frac{d[g : A]}{dt} = \alpha_1[g][A] - \theta_1[g : A], \quad (3)$$

$$g_{\text{tot}} = [g] + [g : M] + [g : A], \quad (4)$$

and similarly for the mRNA and protein concentrations

$$\frac{d[r_b]}{dt} = \rho_f[g] + \rho_b[g : A] + \rho_M[g : M] - \delta_r[r_b], \quad (5)$$

$$\frac{d[B]}{dt} = \beta[r_b] - \delta_B[B] - \gamma_+[A][B] + \gamma_-[A : B], \quad (6)$$

$$\frac{d[A]}{dt} = \rho_A - \gamma_+[A][B] - \delta_A[A] + \theta_1[g : A] - \alpha_1[g][A] + \gamma_-[A : B], \quad (7)$$

$$\frac{d[A : B]}{dt} = \gamma_+[A][B] - \gamma_-[A : B] - \delta_{AB}[A : B]. \quad (8)$$

For the remainder of this section we use the same non-dimensionalization procedure as François and Hakim to derive a dimensionless form of equations Eqs. (1) to (8). Let \tilde{t} be the dimensionless time $\tilde{t} := \delta_r t$ and write $\tilde{u} := \frac{du}{d\tilde{t}}$ for $u \in C^1(\mathbb{R})$, a function of dimensionless time. We normalize the promoter states so that $g_{\text{tot}} = 1$ and obtain dimensionless equations for their time evolution

$$\dot{g} = \tilde{\theta}_1 \left((1 - g - g_M) + \frac{\tilde{\theta}_2}{\tilde{\theta}_1} g_M - g \frac{A}{A_0} \right) - \tilde{\alpha}_2 g, \quad (9)$$

$$\dot{g}_M = \tilde{\alpha}_2 g - \tilde{\theta}_2 g_M, \quad (10)$$

in which $g = [g]/g_{\text{tot}}$ and $g_M = [g : M]/g_{\text{tot}}$. The dimensionless active promoter concentration $g_A = [g : A]/g_{\text{tot}}$ is given by $g_A = 1 - g - g_M$. We rescale the protein concentrations so that $A = \sqrt{\gamma_+/\rho_A}[A]$, $B = \sqrt{\gamma_+/\rho_A}[B]$, $A_B = \sqrt{\gamma_+/\rho_A}[A : B]$, $r = \sqrt{\gamma_+/\rho_A}[r_b]$ to obtain

$$\dot{r} = \rho_0 g + \rho_1 (1 - g - g_M) + \rho_2 g_M - r, \quad (11)$$

$$\dot{A} = \frac{1}{\delta} (1 - A \cdot B) - d_a A + \tilde{K}_d A_B + \mu \tilde{\theta}_1 \left((1 - g - g_M) - g \frac{A}{A_0} \right), \quad (12)$$

$$\dot{B} = \frac{1}{\delta} (r - A \cdot B) - d_b B + \tilde{K}_d A_B, \quad (13)$$

$$\dot{A}_B = \frac{A \cdot B}{\delta} - d_{AB} A_B. \quad (14)$$

Altogether, the IT-MFL model consists of the six dynamic variables g, g_M, r, A, B, A_B that evolve according to Eqs. (9) to (14) and 13 dimensionless parameters: $\rho_0 = \frac{\beta \rho_f}{\rho_A \delta_r}$,

$\rho_1 = \frac{\beta \rho_b}{\rho_A \delta_r}$, $\tilde{\theta}_1 = \frac{\theta_1}{\delta_r}$, $\delta = \frac{\delta_r}{\sqrt{\rho_A \gamma_+}}$, $d_a = \frac{\delta_A}{\delta_r}$, $d_b = \frac{\delta_B}{\delta_r}$, $d_{AB} = \frac{\delta_{AB}}{\delta_r}$, $\mu = \sqrt{\frac{\gamma_+}{\rho_A}}$, $A_0 = \frac{\theta}{\alpha} \sqrt{\frac{\gamma_+}{\rho_A}}$, $\tilde{K}_d = \frac{K_d \gamma_+}{\delta_r}$, $\tilde{\alpha}_2 = \frac{\alpha_2}{\delta_r}$, $\tilde{\theta}_2 = \frac{\theta_2}{\delta_r}$, and $\rho_2 = \frac{\beta \rho_M}{\rho_A \delta_r}$. The last three parameters are new to the IT-MFL model. We will be most interested in the transcription rates ρ_0 , ρ_1 , ρ_2 , the methylation and demethylation rates $\tilde{\alpha}_2$, $\tilde{\theta}_2$, and the timescale ratio δ . Aside from the nonlinearity introduced by the sequestration of A by B , the dynamics of the MFL and IT-MFL models are linear. This weak nonlinearity has made the MFL model attractive for stochastic extensions [25].

III. ANALYSIS

All results in this section which depend on the assumption that the new promoter state is intermediate ($\rho_0 < \rho_2 < \rho_1$) will say so explicitly. Our aim is to determine how the intermediate promoter state affects the stability and period of the IT-MFL model. Building on the work of François and Hakim, we begin by expanding the system perturbatively in δ . This reveals that in the small δ regime, the behavior of the MFL and IT-MFL models are qualitatively similar provided that

$$\rho_0 < \rho_2 < \rho_1. \quad (15)$$

Notice that Eq. (15) is equivalent to the requirement $\rho_f < \rho_M < \rho_b$ because all three transcription rates were rescaled by a factor of $\beta/\rho_A \delta_r$ to arrive at the dimensionless rates. Expressions of the form $1 < \rho_1$ and $\rho_0 < 1$ appear later in this section. Such conditions are naturally interpreted as timescale separations when written in terms of dimensionful parameters. For instance, $\rho_0 < 1$ is equivalent to $\beta \rho_f / \delta_r < \rho_A$ and the second expression is easily interpreted as a comparison between the timescales of B production and A production.

In the later part of this section, we focus on the circadian setting and explicitly show how the Kim-Forger model can be derived from the IT-MFL model. We also relax an assumption commonly employed in this derivation and explore the consequences of this choice. In its reduced form, the IT-MFL model is a monotone cyclic feedback system and therefore obeys a generalization of the Poincaré-Bendixson theorem in this regime. This structure plays a key role in our bifurcation analysis of the reduced model. Using parametric sensitivity analysis, we show that, although the period is not particularly sensitive to the methylation parameters, they do play a non-trivial role in determining the sensitivity of the period to the other parameters in the model. In general, the period becomes most sensitive as the model approaches a Hopf bifurcation rendering its equilibrium stable.

A. Equilibrium uniqueness conditions

The assumption that A is an activator ($\rho_0 < \rho_1$) eliminates the possibility for multistability in the MFL model. François and Hakim showed this by reducing the equilibrium equations of the MFL model to

$$1 = \delta d_a A + \frac{A(\rho_1 A + \rho_0 A_0)}{(A + A_0)(A + \delta d_b)}. \quad (16)$$

The right-hand side of Eq. (16) vanishes when $A = 0$, tends to infinity as $A \rightarrow \infty$, and is monotonic in A when $\rho_0 < \rho_1$. It follows that there is a unique nonnegative value of A that sat-

isfies Eq. (16) and determines the steady state of the system. A similar property is true of the IT-MFL model. We find that at steady state, Eqs. (9) to (14) reduce to

$$1 = \delta d_a A + \frac{A(1 - \frac{\tilde{K}_d^2}{d_{AB}^2})[\rho_1 A + (\rho_0 + \frac{\rho_2 \tilde{\alpha}_2}{\tilde{\theta}_2})A_0]}{[A + A_0(1 + \frac{\tilde{\alpha}_2}{\tilde{\theta}_2})][A + \delta d_b(1 + \frac{\tilde{K}_d}{d_{AB}})]}. \quad (17)$$

Note that Eq. (16) is recovered from Eq. (17) in the limit of no methylation ($\frac{\tilde{\alpha}_2}{\tilde{\theta}_2} \rightarrow 0$) and tight activator-target binding ($\tilde{K}_d \rightarrow 0$). If we assume the additional promoter state has an intermediate transcription rate ($\rho_0 < \rho_2 < \rho_1$) then the right-hand side of Eq. (17) is monotonic in A and there remains a unique nonnegative solution to the system's equilibrium equation.

When the conditions for a unique nonnegative equilibrium are not satisfied, one can proceed algebraically or perturbatively. The algebraic approach taken by Nagy produces a closed-form parametrization of the boundary between unique and multiple equilibria in the parameter space of the MFL model [26,27]. Although this approach still applies to the IT-MFL model, the expressions are more cumbersome and do not give much intuition on differences in the stability boundary in the two models. On the other hand, the perturbative approach taken by François and Hakim is informative when applied to the IT-MFL model. Observe that Eq. (17) can be expanded perturbatively in δ . Using the method of dominant balance [28], we find that A may take low, medium, or high steady-state values

$$A_1 := \delta \frac{d_b(1 + \frac{\tilde{\alpha}_2}{\tilde{\theta}_2})(1 + \frac{\tilde{K}_d}{d_{AB}})}{\rho_0 - 1 + \frac{\tilde{\alpha}_2}{\tilde{\theta}_2}(\rho_2 - 1)} + \mathcal{O}(\delta^2), \quad (18)$$

$$A_2 := \frac{A_0(\rho_0 - 1 + \frac{\tilde{\alpha}_2}{\tilde{\theta}_2}(\rho_2 - 1))}{1 - \rho_1} + \mathcal{O}(\delta), \quad (19)$$

$$A_3 := \frac{1 - \rho_1}{\delta d_a} + \mathcal{O}(1), \quad (20)$$

respectively.

Remark 1. If $\rho_0 < \rho_2 < \rho_1$ then exactly one of the steady states given in Eqs. (18) to (20) will be nonnegative at dominant order. In the particular case where $\rho_0 < 1 < \rho_2$, it cannot be determined a priori which of the three steady states is nonnegative at dominant order.

Remark 1 clarifies how the existence of three steady states relates to the monostability condition $\rho_0 < \rho_2 < \rho_1$. See the Supplemental Material at [29] for further details and a proof of Remark 1. Also, note that the equilibrium solutions in Eqs. (18) to (20) reduce to those found by François and Hakim in the no methylation and tight activator-target binding limit ($\tilde{K}_d \rightarrow 0$). The ratio $\tilde{\alpha}_2/\tilde{\theta}_2 = \alpha_2/\theta_2$ appearing in Eqs. (18) to (20) is the equilibrium constant of the methylation reaction. We denote this value by K_2 and note that a larger value of K_2 corresponds to a stronger presence of methylation in the model. Some intuition can be gained by examining how the steady-state activator concentrations depend on K_2 . As might be expected, ρ_1 is the only transcription rate that influences the high- A steady state A_3 . The remaining parameters in Eq. (18) compare timescales of A production to timescales of B production, but indeed these are independent of methyla-

TABLE I. Steady states and eigenvalues corresponding to the linearization of the MFL and IT-MFL models at the $A_{\text{eq}} = A_2$ steady state. ω_i denotes the i th cubic root of unity for $i = 1, 2, 3$. The additional eigenvalues in the IT-MFL model will be negative provided that $\rho_0 < \rho_2 \leq \rho_1$.

	Steady state	Eigenvalues
MFL	$g_{\text{eq}}^{\text{MFL}} = \frac{A_0}{A_{\text{eq}} + A_0}$ $B_{\text{eq}}^{\text{MFL}} = \frac{\rho_1 A_{\text{eq}} + \rho_0 A_0}{(A_{\text{eq}} + A_0)(A_{\text{eq}} + \delta d_b)}$	$\lambda_i^{\text{MFL}} = -\omega_i \left(\frac{\tilde{\theta}_1 g_{\text{eq}}^{\text{MFL}} A_{\text{eq}} (\rho_1 - \rho_0)}{\delta A_0 (A_{\text{eq}} + B_{\text{eq}}^{\text{MFL}})} \right)^{\frac{1}{3}} + \mathcal{O}(1)$ $\lambda_4^{\text{MFL}} = \frac{-(A_{\text{eq}} + B_{\text{eq}}^{\text{MFL}})}{\delta} + \mathcal{O}(1)$
IT-MFL	$g_{\text{eq}}^{\text{IT-MFL}} = \frac{A_0}{A_{\text{eq}} + A_0(1 + \frac{\tilde{\alpha}_2}{\tilde{\theta}_2})}$ $B_{\text{eq}}^{\text{IT-MFL}} = \frac{(1 + \frac{\tilde{\kappa}_d}{d_{AB}})[\rho_1 A_{\text{eq}} + (\rho_0 + \frac{\rho_2 \tilde{\alpha}_2}{\tilde{\theta}_2})A_0]}{[A_{\text{eq}} + A_0(1 + \frac{\tilde{\alpha}_2}{\tilde{\theta}_2})][A_{\text{eq}} + \delta d_b(1 + \frac{\tilde{\kappa}_d}{d_{AB}})]}$	$\lambda_i^{\text{IT-MFL}} = -\omega_i \left(\frac{\tilde{\theta}_1 g_{\text{eq}}^{\text{IT-MFL}} A_{\text{eq}} (\rho_1 - \rho_0)}{\delta A_0 (A_{\text{eq}} + B_{\text{eq}}^{\text{IT-MFL}})} \right)^{\frac{1}{3}} + \mathcal{O}(1)$ $\lambda_4^{\text{IT-MFL}} = \frac{-(A_{\text{eq}} + B_{\text{eq}}^{\text{IT-MFL}})}{\delta} + \mathcal{O}(1)$ $\lambda_5^{\text{IT-MFL}} = \frac{(1 + \frac{\tilde{\alpha}_2}{\tilde{\theta}_2})\rho_1 - (\rho_0 + \frac{\tilde{\alpha}_2}{\tilde{\theta}_2})\rho_2}{\frac{1}{\tilde{\theta}_2}(\rho_0 - \rho_1)} + \mathcal{O}(\delta)$ $\lambda_6^{\text{IT-MFL}} = -d_{AB} + \mathcal{O}(\delta)$

tion. The low and medium steady-state concentrations (A_1 and A_2), on the other hand, are influenced by methylation. Under the standard assumption that the methylated promoter state has an intermediate transcription rate ($\rho_2 < \rho_1$), one finds that the lowest steady-state (A_1) is decreasing as a function of K_2 . The case for A_2 is similar, except one requires instead that $(1 - \rho_2)/(\rho_1 - 1) > 0$, or equivalently $\rho_2 < 1 < \rho_1$. The interpretation of such expressions in terms of dimensionful parameters is discussed in the next section. One might expect that the incorporation of methylation in the model could result in a lower concentration of the target protein (B) in the system, hence less sequestration, and therefore more free activator. Our analysis reveals that the opposite is true under reasonable conditions on the parameters.

B. Linear stability analysis

We now focus on the case where A is an activator and the new promoter state is intermediate ($\rho_0 < \rho_2 < \rho_1$). From the previous section, we know there is a unique nonnegative equilibrium $A_{\text{eq}} = A_2$ in this case. We use the subscript “eq” to refer to the steady-state value of a dynamic variable corresponding to the equilibrium $A(t) = A_{\text{eq}}$. When linearized at A_{eq} , we see in Table I that the dominant-order terms in the eigenvalues of the MFL and IT-MFL models are most easily compared when expressed in terms of the g and B steady states. The first row of Table I summarizes the findings of François and Hakim and the second row contains our extension of their calculations. Both models possess eigenvalues proportional to each of the cubic roots of unity, along with an eigenvalue λ_4 which is stable for all parameter values.

Two additional eigenvalues are present in the IT-MFL model. Under the assumption that $\rho_0 < \rho_2 \leq \rho_1$, we can show the $\lambda_5^{\text{IT-MFL}}$ eigenvalue is stable at dominant order.

Proposition 1. If $\rho_0 < \rho_2 \leq \rho_1$ then $\lambda_5^{\text{IT-MFL}} < 0$ to dominant order as $\delta \rightarrow 0$.

See the Supplemental Material at [29] for a proof of Proposition 1. The other new eigenvalue $\lambda_6^{\text{IT-MFL}}$ is always stable to dominant order since $d_{AB} \geq 0$. We see that the qualita-

tive behavior (the linear stability and number of nonnegative equilibria) is similar between the MFL and IT-MFL models provided that $\rho_0 < \rho_2 < \rho_1$. A natural extension of this work would be to see if this phenomenon persists in n -promoter state models.

C. Period estimation

Oscillatory solutions of the MFL model oscillate between phases of high- A -low- B and low- A -high- B concentration. Such phases are referred to as Phases I and II of the limit cycle, respectively. The boundary layer structure of these oscillations (schematized in Fig. 2) is crucial for François and Hakim’s original estimates of the model’s period. The numerical simulations in Fig. 3 show it is possible to change the period of the IT-MFL model by only altering the methylation parameters. To analyze such solutions, we use the same technique as François and Hakim. We make a change of variable $A \rightarrow \delta a$ for the Phase I of the limit cycle and $B \rightarrow \delta b$ for Phase II. Following this substitution, we approximate the governing equations to lowest nontrivial order in δ . In this approximation, some variables are left in the steady state and others obey linear differential equations. The steady-state values and linear equations for each of the two phases are summarized in the first two rows of Table II. Imposing continuity of the solution across the boundary layers, depicted in Fig. 2, produces a system of nonlinear equations that determines the constants of integration and the durations of each phase. For both models, the system of nonlinear equations can be separated into boundary conditions and a closed system of equations implicitly determining the period. These systems are listed in the third and fourth rows of Table II.

When the influence of the smaller boundary layers are included, the $\mathcal{O}(\delta^0)$ period estimate is improved to an $\mathcal{O}(\sqrt{\delta})$ estimate. These corrections result in updated boundary conditions and an updated system of nonlinear equations, given in the final two rows of Table II. Comparing the $\mathcal{O}(\delta^0)$ and $\mathcal{O}(\sqrt{\delta})$ estimates, we see that the only change in boundary conditions is for the $g_{II}(t)$ solution and the only change in

TABLE II. Summary of the nonlinear equations derived in the lowest-order and dominant-order period estimates. Phases I and II of the oscillations are defined in Fig. 2 and shown for a nominal simulation in Fig. 3. The rescaled variables are given by $a := \delta A$ and $b := \delta B$ and the parameters $\kappa_1 := \frac{\tilde{\theta}_1(1-r_1)}{2A_0\delta}$ and $g_1 := 1 - e^{-\tilde{\theta}_1 t_2}$.

	MFL	IT-MFL
Phase I	$g = \frac{\delta A_0}{a}$ $B = \frac{\delta r}{a}$ $\dot{r} = \rho_1 - r$ $\dot{a} = 1 - r - d_a a$	$g = \frac{\delta A_0}{a} \left[1 - \left(1 - \frac{\tilde{\theta}_2}{\tilde{\theta}_1} \right) g_M \right]$ $B = \frac{\delta r_0}{a}$ $\dot{g}_M = -\tilde{\theta}_2 g_M$ $\dot{r} = \rho_1(1 - g - g_M) + g_M \rho_2 - r$ $\dot{a} = 1 - r - d_a a$
Phase II	$A = \frac{\delta}{b}$ $\dot{g} = \tilde{\theta}_1(1 - g)$ $\dot{r} = \rho_0 g + \rho_1(1 - g) - r$ $\dot{b} = r - 1 - d_b b$	$A = \frac{\delta}{b}$ $\dot{g} = \tilde{\theta}_1 \left(1 - g - g_M + \frac{\tilde{\theta}_2}{\tilde{\theta}_1} g_M \right) - \tilde{\alpha}_2 g$ $\dot{g}_M = \tilde{\alpha}_2 g - \tilde{\theta}_2 g_M$ $\dot{r} = \rho_0 g + \rho_1(1 - g - g_M) + g_M \rho_2 - r$ $\dot{b} = r - 1 - b d_b$
Boundary conditions $\mathcal{O}(\delta^0)$ estimate	$r_I(0) = r_1, \quad a_I(0) = 0,$ $g_{II}(0) = 0, \quad r_{II}(0) = r_2,$ $b_{II}(0) = 0$	$r_I(0) = r_1, \quad a_I(0) = 0, \quad g_{M,I}(0) = g_{M1},$ $g_{II}(0) = 0, \quad g_{M,II}(0) = g_{M2}, \quad r_{II}(0) = r_2,$ $b_{II}(0) = 0$
$\mathcal{O}(\delta^0)$ Estimate	$r_I(t_1) = r_2, \quad a_I(t_1) = 0,$ $r_{II}(t_2) = r_1, \quad b_{II}(t_2) = 0$	$r_I(t_1) = r_2, \quad a_I(t_1) = 0, \quad g_{M,I}(t_1) = g_{M2},$ $r_{II}(t_2) = r_1, \quad b_{II}(t_2) = 0, \quad g_{M,II}(t_2) = g_{M1}$
Boundary conditions $\mathcal{O}(\sqrt{\delta})$ estimate	$r_I(0) = r_1, \quad a_I(0) = 0,$ $g_{II}(0) = \sqrt{\frac{\pi A_0 \tilde{\theta}_1 \delta}{2(r_2 - 1)}}, \quad r_{II}(0) = r_2,$ $b_{II}(0) = 0$	$r_I(0) = r_1, \quad a_I(0) = 0, \quad g_{M,I}(0) = g_{M1},$ $g_{II}(0) = (\tilde{\theta}_1 + (\tilde{\theta}_2 - \tilde{\theta}_1) g_{M2}) \sqrt{\frac{\pi A_0 \delta}{2\tilde{\theta}_1(r_2 - 1)}},$ $g_{M,II}(0) = g_{M2}, \quad r_{II}(0) = r_2,$ $b_{II}(0) = 0$
$\mathcal{O}(\sqrt{\delta})$ Estimate	$r_I(t_1) = r_2, \quad a_I(t_1) = 0,$ $r_{II}(t_2) = r_1 + g_1(\rho_1 - \rho_0) \sqrt{\frac{\pi}{4\kappa_1}},$ $b_{II}(t_2) = 0$	$r_I(t_1) = r_2, \quad a_I(t_1) = 0, \quad g_{M,I}(t_1) = g_{M2},$ $r_{II}(t_2) = r_1 + g_1(\rho_1 - \rho_0) \sqrt{\frac{\pi}{4\kappa_1}},$ $b_{II}(t_2) = 0, \quad g_{M,II}(t_2) = g_{M1}$

the period equations is for $r_{II}(t)$. Even in the case of the $\mathcal{O}(\delta^0)$ estimate in the MFL model, the system of implicit equations given in Table II cannot be solved exactly. Figure 4 shows a strong agreement between a fully numerical simulation and a numerical solution of the nonlinear system of equations from Table II.

Continuing to follow the methodology of François and Hakim, we make two additional simplifying assumptions to obtain approximate expressions for the $\mathcal{O}(\delta^0)$ period estimate. First, we assume the decay rate of B is smaller than the decay rate of its mRNA. Second, we assume the transcription rate corresponding to the active promoter state is larger than the expression rate of A . When expressed in terms of the

model parameters, these two assumptions give us $d_b = 0$ and $\rho_1 \gg 1$. When $d_b = 0$, the expressions for the solutions in each phase of the limit cycle become much simpler. Under the assumption $\rho_1 \gg 1$, it is justifiable to Taylor expand the system of implicit equations in powers of $\frac{1}{\rho_1}$. In addition, it can be verified by simulation and later confirmed by the approximate formulas in Table III that t_1 decreases as ρ_1 increases. This allows us to also Taylor expand the implicit equations in powers of t_1 . Table III summarizes the result of Taylor expanding the implicit equations from the $\mathcal{O}(\delta^0)$ estimate from Table II in powers of $\frac{1}{\rho_1}$ and t_1 , and neglecting any terms that are exponentially small in t_2 . See the Supplemental Material at [29] for further details on this calculation. Figure 5 shows

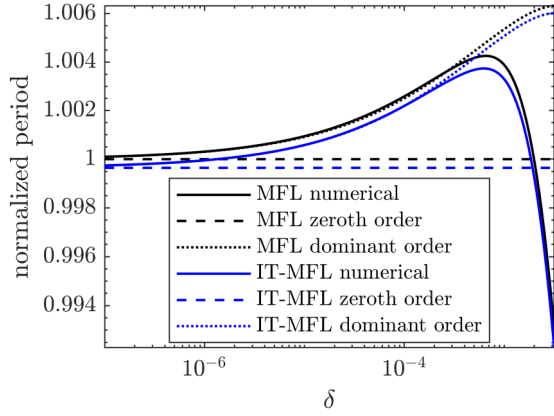


FIG. 4. Comparison of numerically and asymptotically estimated periods. The period is expressed as a ratio with its limiting value as $\delta \rightarrow 0$. Parameters for the intermediate promoter state were selected so its influence is weak ($\rho_2 = 0$, $\tilde{\alpha}_2 \ll \tilde{\theta}_2$). Parameters: $\rho_0 = 0$, $\rho_1 = 10.45$, $\tilde{\theta}_1 = 1.33$, $d_a = 0.33$, $d_b = 0.33$, $\mu = 0.31$, $A_0 = 4$, $\rho_2 = 0$, $\tilde{\alpha}_2 = 1.0$, $\tilde{\theta}_2 = 10$.

reasonable agreement between numerical period estimation and the approximate expressions from Table III. Since we have Taylor expanded in powers of $\frac{1}{\rho_1}$, note that we expect to see agreement as ρ_1 gets large in Fig. 5.

Comparing the MFL and IT-MFL period estimates, it is immediate that t_1 is always larger in the IT-MFL model and that its contribution to the period vanishes as $\rho_1 \rightarrow \infty$. Hence in the large ρ_1 limit, the period is approximately equal to t_2 . The following two remarks give some interpretation to the extra terms that appear in the expression for t_2 in the case of the IT-MFL model.

Remark 2. t_2 depends linearly on ρ_1 with a slope given by

$$\frac{\partial t_2^{\text{MFL}}}{\partial \rho_1} = \frac{1}{\tilde{\theta}_1(1 - \rho_0)}, \quad (21)$$

$$\frac{\partial t_2^{\text{IT-MFL}}}{\partial \rho_1} = \frac{1}{\tilde{\theta}_1(1 - \rho_0 + \frac{\tilde{\alpha}_2}{\tilde{\theta}_2}(1 - \rho_2))(1 + \frac{\tilde{\alpha}_2}{\tilde{\theta}_2})}. \quad (22)$$

TABLE III. Limiting value of period estimate for MFL and IT-MFL models.

Equation	MFL	IT-MFL
$a_I(t_1) = 0$	$t_1 = \frac{2(1-\rho_0)}{\rho_1}$	$t_1 = \frac{2(1-\rho_0)}{\rho_1} + \frac{2(1-\rho_2)\frac{\tilde{\alpha}_2}{\tilde{\theta}_2}}{\rho_1}$
$r_I(t_1) = r_2$	$r_2 = 2 - \rho_0$	$r_2 = \frac{2 - \rho_0 + (2 - \rho_2)\frac{\tilde{\alpha}_2}{\tilde{\theta}_2}}{1 + \frac{\tilde{\alpha}_2}{\tilde{\theta}_2}}$
$r_{II}(t_2) = r_1$	$r_1 = \rho_0$	$r_1 = \frac{\rho_0 + \rho_2\frac{\tilde{\alpha}_2}{\tilde{\theta}_2}}{1 + \frac{\tilde{\alpha}_2}{\tilde{\theta}_2}}$
$b_{II}(t_2) = 0$	$t_2 = 2 + \frac{\rho_1 - \rho_0}{\tilde{\theta}_1(1 - \rho_0)}$	$t_2 = 2 + \frac{\rho_1 - \rho_0 + \frac{\tilde{\alpha}_2}{\tilde{\theta}_2}(\rho_1 - \rho_2)}{\tilde{\theta}_1(1 - \rho_0 + (1 - \rho_2)\frac{\tilde{\alpha}_2}{\tilde{\theta}_2})(1 + \frac{\tilde{\alpha}_2}{\tilde{\theta}_2})}$
$g_{M,I}(t_1) = g_{M2}$	N/A	$g_{M2} = \frac{\tilde{\alpha}_2}{\tilde{\alpha}_2 + \tilde{\theta}_2}$
$g_{M,II}(t_2) = g_{M1}$	N/A	$g_{M1} = \frac{\tilde{\alpha}_2}{\tilde{\alpha}_2 + \tilde{\theta}_2}$

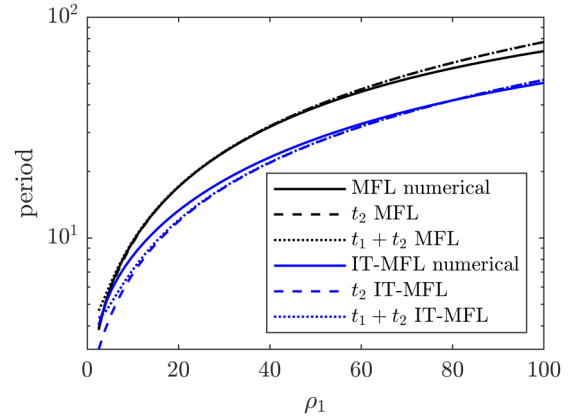


FIG. 5. Comparison of numerically estimated period and the limiting values given in Table III. We see $t_2^{\text{IT-MFL}} < t_2^{\text{MFL}}$ when ρ_1 is large, as proved in Remark 2. Simulation parameters: $\delta = 10^{-4}$, $\rho_0 = 0$, $\tilde{\theta}_1 = 1.33$, $d_a = 0.3$, $d_b = 0$, $\mu = 0.31$, $A_0 = 4$, $\rho_2 = 0.5$, $\tilde{\alpha}_2 = 1$, $\tilde{\theta}_2 = 1$.

In the case that $\rho_0 < 1$ and $\rho_2 < 1$, both t_2^{MFL} and $t_2^{\text{IT-MFL}}$ are monotonically increasing in ρ_1 with

$$\frac{\partial t_2^{\text{IT-MFL}}}{\partial \rho_1} \leq \frac{\partial t_2^{\text{MFL}}}{\partial \rho_1}. \quad (23)$$

An expression of the form $1 - \rho_0 > 0$ may be rewritten in dimensionful parameters as $\delta_r \rho_A > \beta \rho_f$. So we see the sign and magnitude of our approximation for the slope are determined by how the timescales of activator and target production compare to one another. Also note that the right-hand side of Eq. (22) becomes larger or smaller relative to the corresponding expression in the MFL model in Eq. (21) depending on if $\rho_2 < 1$ or $\rho_2 > 1$.

In the case where $\rho_0 < 1$ and $\rho_2 < 1$, we obtain a stronger result where the period of the IT-MFL model is controlled by the period of the MFL model up to a constant.

Remark 3. If $\rho_0 < 1$, $\rho_2 < 1$, and $\rho_1 > \max(\rho_0, \rho_2)$ then

$$t_2^{\text{IT-MFL}} \leq t_2^{\text{MFL}} + C, \quad (24)$$

with $C = \frac{\rho_1 - \rho_2}{\tilde{\theta}_1} \min(\frac{\tilde{\alpha}_2}{\tilde{\theta}_2(1 - \rho_0)}, \frac{1}{1 - \rho_2})$.

See the Supplemental Material at [29] for a proof of Remark 3. One can interpret these results as follows: in the current approximation, $t_2^{\text{IT-MFL}} < t_2^{\text{MFL}}$ when ρ_1 is large enough by Remark 2, and although we may find $t_2^{\text{MFL}} < t_2^{\text{IT-MFL}}$ for moderate ρ_1 , this is controlled by the constant C given in Remark 3.

D. Relation between the Kim-Forger, Goodwin, MFL, and IT-MFL models

So far our analysis has been an extension of the original MFL paper of François and Hakim. We now shift our attention to the work of Kim and Forger. The Kim-Forger model is a three-dynamic-variable negative feedback loop with nonlinearity introduced by means of a sequestration function [22]

$$f(P; A, K_d) = \frac{1}{2}(1 - P/A - K_d/A + \sqrt{(1 - P/A - K_d/A)^2 + 4K_d/A}), \quad (25)$$

with governing equations of the form

$$\frac{dM}{dt} = \alpha_1 f(P) - \beta_1 M, \quad (26)$$

$$\frac{dP_c}{dt} = \alpha_2 M - \beta_2 P_c, \quad (27)$$

$$\frac{dP}{dt} = \alpha_3 P_c - \beta_3 P. \quad (28)$$

Kim and Forger interpret M , P_c , and P as the mRNA, cytosolic, and nuclear concentrations of the target protein PER. The parameter A in Eq. (25) represents the total concentration of activator CLOCK-BMAL1 and K_d is the dissociation constant of the activator-target binding reaction. The aim of this section is to explain how one can start with the MFL model and arrive at the Kim-Forger model. We also discuss how the standard assumptions can be relaxed to provide a better approximation of the IT-MFL model.

In the context of the MFL model, Eqs. (26) to (28) can be obtained as a consequence of the following assumptions: The transcription rate corresponding to the inactive promoter state is zero, the binding of A and B has reached equilibrium (rapid equilibrium approximation), the total amount of activator A_{tot} is constant, the transcription rate of P is proportional to the fraction of unbound activator $f = \frac{A}{A_{\text{tot}}}$, and finally that the QSS values of A and the promoter states are decoupled. By adding nuclear export and import of the target protein to the MFL model and applying the assumptions listed above, one may reduce the MFL model to Eqs. (26) to (28). In particular, if one begins with the full MFL model and follows the reduction stated above, the following reduced model is obtained as follows:

$$\frac{d[r_b]}{dt} = \rho_b K_1 g_{\text{tot}} A_{\text{tot}} f([B_{\text{tot}}]; A_{\text{tot}}, K_d) - \delta_r [r_b], \quad (29)$$

$$\frac{d[B_c]}{dt} = \beta_1 [r_b] - \lambda_c [B_c], \quad (30)$$

$$\frac{d[B_{\text{tot}}]}{dt} = \beta_2 [r_b] - \delta_B [B_{\text{tot}}], \quad (31)$$

in which $K_1 = \alpha_1/\theta_1$ and $K_d = \gamma_-/\gamma_+$. See the Supplemental Material at [29] for a detailed derivation of Eqs. (29) to (31). Notice that under the mapping $[r_b] \rightarrow M$, $[B_c] \rightarrow P_c$, $[B_{\text{tot}}] \rightarrow P$, and relabelling of parameters, Eqs. (29) to (31) are identical with the version of the Kim Forger model stated in Eqs. (26) to (28). One should be cautious in viewing Eqs. (26) to (28) [or equivalently Eqs. (29) to (31)] as a reduction of the MFL model since their derivation requires adding nuclear import and export to the model, thereby introducing a new dynamic variable: the cytosolic PER concentration. Naturally, the same is true of the IT-MFL model when we perform a similar reduction to obtain Eqs. (37) to (39). We refer to the reduction of Kim and Forger as “artificially decoupled” because the steady-state value of $[A]$ in their reduced model can be obtained by decoupling $[A]$ from the equilibrium of the promoter states. Our approximation of the IT-MFL model starts instead with the fully coupled set of equilibrium equations and produces a cubic equation $\Phi_{\text{dim}}([A]_{\text{qss}}) = 0$ for the QSS concentration $[A]_{\text{qss}}$, where Φ_{dim} is given by

$$\Phi_{\text{dim}}([A]) = a_{\text{dim}}[A]^3 + b_{\text{dim}}[A]^2 + c_{\text{dim}}[A] + d_{\text{dim}}, \quad (32)$$

with coefficients

$$a_{\text{dim}} = K_1, \quad (33)$$

$$b_{\text{dim}} = 1 + K_2 + (g_{\text{tot}} + B_{\text{tot}} - A_{\text{tot}} + K_d)K_1, \quad (34)$$

$$c_{\text{dim}} = (1 + K_2)(B_{\text{tot}} - A_{\text{tot}} + K_d) + (g_{\text{tot}} - A_{\text{tot}})K_d K_1, \quad (35)$$

$$d_{\text{dim}} = -(1 + K_2)A_{\text{tot}}K_d, \quad (36)$$

and the equilibrium constants are given by $K_1 = \alpha_1/\theta_1$ and $K_2 = \alpha_2/\theta_2$, the dissociation constant $K_d = \gamma_-/\gamma_+$, A_{tot} is constant by assumption, and $B_{\text{tot}} = [B_{\text{tot}}]$. See the Supplemental Material at [29] for a derivation and analysis of $\Phi_{\text{dim}}([A])$. We emphasize that this polynomial is dimensionful because its dimensionless form, which we denote simply by $\Phi(\tilde{A})$, appears in the Supplemental Material. We denote the solution to $\Phi_{\text{dim}}([A]) = 0$ by $[A]_{\text{qss}}$ and obtain a reduced form of the IT-MFL model

$$\frac{d[r_b]}{dt} = \rho_b [g : A]_{\text{qss}} + \rho_M [g : M]_{\text{qss}} - \delta_r [r_b], \quad (37)$$

$$\frac{d[B_c]}{dt} = \beta_1 [r_b] - \lambda_c [B_c], \quad (38)$$

$$\frac{d[B_{\text{tot}}]}{dt} = \beta_2 [B_c] - \delta_B [B_{\text{tot}}], \quad (39)$$

in which $[B_c]$ is the concentration of cytosolic protein and the promoter states $[g : A]_{\text{qss}}$ and $[g : M]_{\text{qss}}$ can be expressed in terms of $[A]_{\text{qss}}$ as

$$[g : A]_{\text{qss}} = \frac{[A]_{\text{qss}} K_1 g_{\text{tot}}}{1 + K_2 + [A]_{\text{qss}} K_1}, \quad (40)$$

$$[g : M]_{\text{qss}} = \frac{K_2 (g_{\text{tot}} - [g : A]_{\text{qss}})}{1 + K_2}. \quad (41)$$

Of all the assumptions involved in the derivation of Eqs. (37) to (41), the assumption of $[A]_{\text{tot}}$ being constant in time seems to be the most difficult to verify. Supplemental Fig. 1 shows that the IT-MFL model is well approximated by Eqs. (37) to (41) provided that $[A]_{\text{tot}}$ is close to constant in time and the other assumptions used in the model reduction hold true. Following a non-dimensionalization scheme similar to that of Kim and Forger, we reduce Eqs. (37) to (39) to

$$\frac{d\tilde{r}}{d\tau} = T(\tilde{B}_{\text{tot}}) - \tilde{r}, \quad (42)$$

$$\frac{d\tilde{B}_c}{d\tau} = \tilde{r} - \tilde{B}_c, \quad (43)$$

$$\frac{d\tilde{B}_{\text{tot}}}{d\tau} = \tilde{B}_c - \tilde{B}_{\text{tot}}, \quad (44)$$

$$T(\tilde{B}_{\text{tot}}) = \left(\frac{\tilde{A}_{\text{qss}}(\tilde{B}_{\text{tot}})\tilde{K}_1}{1 + K_2 + \tilde{A}_{\text{qss}}(\tilde{B}_{\text{tot}})\tilde{K}_1} \right) \left(1 - \frac{\rho K_2}{1 + K_2} \right) + \frac{\rho K_2}{1 + K_2}. \quad (45)$$

in which $\tau = t\delta_r$ and $[A]_{\text{qss}} = B^* \tilde{A}_{\text{qss}}(\tilde{B}_{\text{tot}})$. We show in the Supplemental Material that $\tilde{A}_{\text{qss}}(\tilde{B}_{\text{tot}})$ is a root of the polynomial $\Phi(\tilde{A})$ mentioned earlier in this section [29]. The

dimensionless concentrations \tilde{r} , \tilde{B}_c , \tilde{B} satisfy

$$[r_b] = r_b^* \tilde{r}, \quad [B_c] = B_c^* \tilde{B}_c, \quad B_{\text{tot}} = B^* \tilde{B}_{\text{tot}}, \quad (46)$$

with scaling factors

$$r_b^* = \frac{\rho_b g_{\text{tot}}}{\delta_r}, \quad B_c^* = \frac{\beta_1 \rho_b g_{\text{tot}}}{\delta_r^2}, \quad B^* = \frac{\beta_2 \beta_1 \rho_b g_{\text{tot}}}{\delta_r^3}, \quad (47)$$

and the dimensionless parameters satisfy

$$\rho = \frac{\rho_M}{\rho_b}, \quad K_2 = \frac{\alpha_2}{\theta_2}, \quad \tilde{K}_1 = B^* K_1 = B^* \frac{\alpha_1}{\theta_1}, \quad (48)$$

$$\tilde{K}_d = \frac{K_d}{B^*}, \quad \tilde{A}_{\text{tot}} = B^* \tilde{A}_{\text{tot}}, \quad \tilde{g}_{\text{tot}} = B^* \tilde{g}_{\text{tot}}. \quad (49)$$

To reduce the number of parameters in the dimensionless model, we also assumed all degradation rates are equal ($\delta_r = \lambda_c = \delta_B$). In a sense that is made precise in the work of Forger [30], the assumption of equal degradation rates maximizes the likelihood of periodic behavior in the system. Since our analysis in the next section is concerned with the situation where oscillations cease to exist, we believe this to be a reasonable simplification. Written in its dimensionless form, our reduction of the IT-MFL model contains three dynamic variables \tilde{r} , \tilde{B}_c , and \tilde{B}_{tot} which evolve according to Eqs. (42) to (45) and six parameters \tilde{A}_{tot} , \tilde{g}_{tot} , \tilde{K}_d , ρ , \tilde{K}_1 , and K_2 .

E. Stability and period sensitivity in the reduced IT-MFL model

When the Kim-Forger model is non-dimensionalized using the same procedure as the reduced IT-MFL model, given in Eqs. (46) to (49), a factor of $\tilde{K}_1 \tilde{A}_{\text{tot}}$ remains in front of the transcription function $f(\tilde{B}_{\text{tot}})$. As shown in Fig. 6, this factor can have a substantial effect on the transcription function. Figure 6 also shows that even in the absence of methylation effects, there are substantial differences in the transcription functions of these two models. Importantly, the monotonicity of $f(\tilde{B}_{\text{tot}})$ which is crucial to the analysis of Kim and Forger appears to be preserved when one switches from $f(\tilde{B}_{\text{tot}})$ to $T(\tilde{B}_{\text{tot}})$ in Fig. 6. Under some conditions given in the Supplemental Material, we prove that this is indeed the case [29]. Assuming these conditions hold true, it follows from the monotonicity of $T(\tilde{B}_{\text{tot}})$ that there is a unique nonnegative equilibrium solution to Eqs. (42) to (45). Moreover, we show in the Supplemental Material that the monotonicity conditions also ensure non-negative solutions to Eqs. (42) to (45) are bounded. This implies that the reduced IT-MFL model constitutes a bounded monotone cyclic feedback (MCF) system, so any solution must converge to static equilibrium, a nonconstant periodic solution, or a combination of homoclinic and heteroclinic orbits connecting the previous two types of equilibria. This is a consequence of Mallet-Paret and Smith's generalization of the Poincaré-Bendixson theorem to MCF systems [31]. MCF systems are capable of bistability, for example, the coexistence of a stable equilibrium and a stable periodic solution. The top panel of Fig. 7 shows that the reduced IT-MFL model can display such behavior. Bistability can be eliminated by introducing a moderate amount of methylation into the system, as in the bottom panel of Fig. 7.

To better understand the qualitative influence of methylation in the reduced model, we fix parameters \tilde{A}_{tot} , \tilde{K}_d , and \tilde{g}_{tot} , and numerically compute the location of any

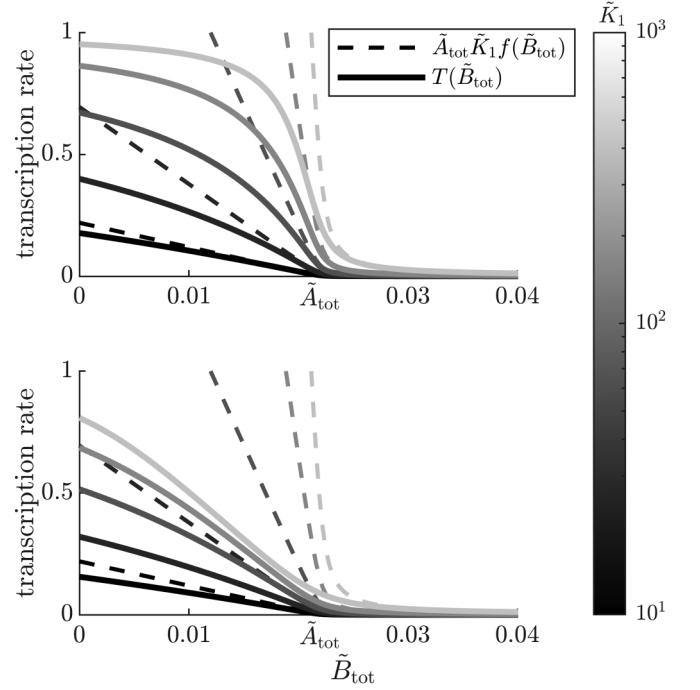


FIG. 6. Comparison of the transcription functions in the dimensionless Kim-Forger and reduced IT-MFL models. The analysis of Kim and Forger shows that $f(\tilde{B}_{\text{tot}})$ has a knee at the value $\tilde{B}_{\text{tot}} = \tilde{A}_{\text{tot}}$, indicated on the \tilde{B}_{tot} axis. (Top panel) \tilde{A}_{tot} is an order of magnitude larger than \tilde{g}_{tot} . As the equilibrium constant \tilde{K}_1 is varied, the transcription function $T(\tilde{B}_{\text{tot}})$ of the reduced IT-MFL model becomes increasingly nonlinear. (Bottom panel) The transcription function in the reduced IT-MFL model resembles a piecewise affine function when \tilde{g}_{tot} and \tilde{A}_{tot} are equal. Null methylation parameters were used in both plots ($\rho = 0 = K_2$) so any difference between the transcription functions should be attributed to the relaxation of Kim and Forger's quasi-steady-state assumption. Parameters: $\tilde{A}_{\text{tot}} = 2.20 \times 10^{-2}$, $\tilde{K}_d = 10^{-5}$, $\rho = K_2 = 0$. In the top panel $\tilde{g}_{\text{tot}} = 2.20 \times 10^{-3}$ and in the bottom $\tilde{g}_{\text{tot}} = 2.20 \times 10^{-2}$.

Hopf bifurcations in the methylation parameters ρ and K_2 . We use pseudoarc-length continuation [32] of the equations $\Phi(\tilde{A}_{\text{qss}}) = 0$, $T(B_{\text{tot}}) = B_{\text{tot}}$ (condition for equilibrium), and $-\frac{1}{2} \sqrt[3]{T'(B_{\text{tot}})} - 1 = 0$ (complex conjugate pair of eigenvalues of the equilibrium's linearization are crossing the imaginary axis) in the unknowns \tilde{A}_{qss} , B_{tot} , ρ , and K_2 . The value of \tilde{K}_1 is varied from 10^{-1} to 10^3 and the result is shown in Fig. 8. These Hopf bifurcations are confirmed to be supercritical by numerically evaluating the first Lyapunov coefficient [33]. Therefore, to the left of each curve, there is a stable periodic solution and an unstable equilibrium. To the right of each curve, there is a single stable equilibrium. Notice the Hopf bifurcation curve disappears for \tilde{K}_1 below a specific value (11.6 for the parameters in Fig. 8) as $K_2 \rightarrow 0$. Also, the reduced IT-MFL exhibits oscillations for sufficiently high \tilde{K}_1 and for sufficiently low methylation parameters ρ and K_2 . These findings do not contradict Fig. 7 because they use different parameters. Repeating the calculations shown in Fig. 8 with the parameters of Fig. 7, we find the Hopf bifurcations could be subcritical or supercritical depending on the value of \tilde{K}_1 , consistent with our observation of bistability.

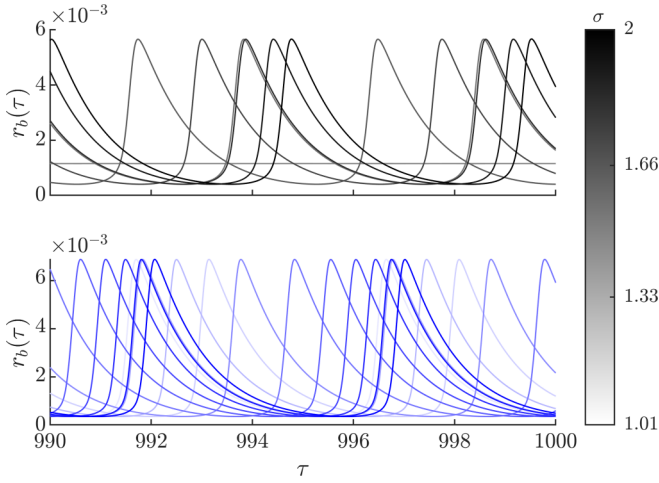


FIG. 7. Methylation can remove bistability from the reduced IT-MFL model. The reduced IT-MFL model was simulated with initial conditions of the form $\sigma \tilde{B}_{\text{tot,eq}} = \tilde{r}_b(0) = \tilde{B}_c(0) = \tilde{B}_{\text{tot}}(0)$ where $\tilde{B}_{\text{tot,eq}}$ is the equilibrium value of \tilde{B}_{tot} and σ takes 11 uniform values in $[1.01, 2]$. (Top) After an initial transient, solutions settle to either periodic or constant trajectories. (Bottom) All solutions settle to periodic trajectories due to the moderate amount of methylation. Parameters: $\tilde{A}_{\text{tot}} = 10^{-3}$, $\tilde{K}_d = 10^{-6.75}$, $\tilde{K}_1 = 10^3$, $\tilde{g}_{\text{tot}} = 10^{-4}$, $\rho = 0$. $K_2 = 0$ in the top panel and $K_2 = 0.12$ in the bottom panel.

The influence of the methylation parameters on the location of the Hopf bifurcation can also be observed when one performs parametric sensitivity analysis on the period. We use a method of sensitivity analysis intended for oscillating systems [34] which avoids some of the numerical difficulties encountered when studying period sensitivity. The sensitivities of the period with respect to \tilde{A}_{tot} and K_2 are shown in

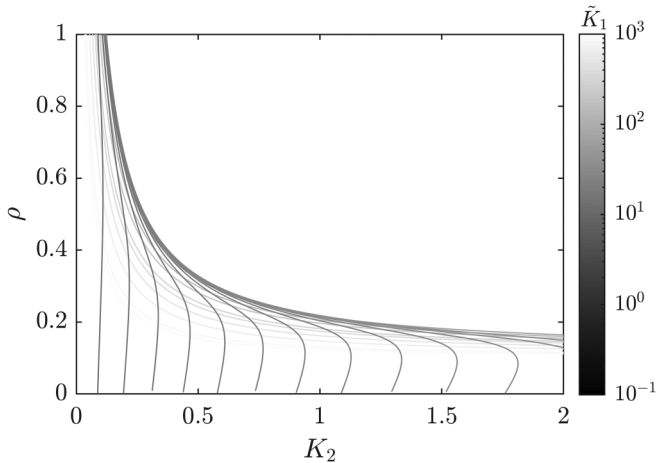


FIG. 8. Each grayscale colored curve corresponds to a Hopf bifurcation in ρ , K_2 . The color gives the value of \tilde{K}_1 . Using the Lyapunov coefficient, we find these bifurcations are supercritical. To the left of each curve there is a stable periodic solution and to the right there is a single stable equilibrium. The other parameters are $\tilde{A}_{\text{tot}} = 1.31 \times 10^{-1}$, $\tilde{g}_{\text{tot}} = 1.31 \times 10^{-2}$, $\tilde{K}_d = 10^{-5}$. This shows that methylation can make the clock arrhythmic. Hopf bifurcations do not occur for \tilde{K}_1 below approximately 11.6 as the bifurcation value of K_2 goes to zero.

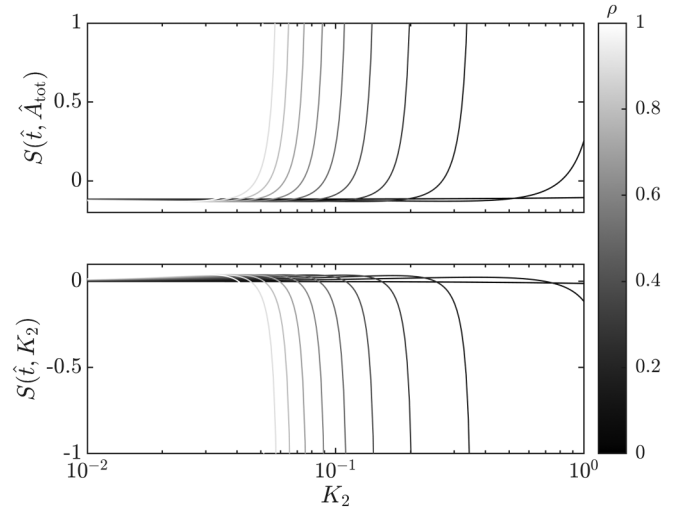


FIG. 9. Numerically computed period sensitivities. $S(\hat{\tau}, p) := \frac{p}{\hat{\tau}} \frac{\partial \hat{\tau}}{\partial p}$ denotes the sensitivity of the period $\hat{\tau}$ with respect to a parameter p , with $p = \tilde{A}_{\text{tot}}$ in the top panel and $p = K_2$ in the bottom panel. The dimensionless transcription rate ρ was varied uniformly from 0 to 1 and this is represented by the transparency of each sensitivity curve. In general, the sensitivities of the period grow as K_2 is increased and the fixed point becomes stable, rendering the model arrhythmic. Simulation parameters $\tilde{A}_{\text{tot}} = 7 \times 10^{-2}$, $\tilde{K}_d = 10^{-6}$, $\tilde{K}_1 = 10^3$, $\tilde{g}_{\text{tot}} = 10^{-3}$.

Fig. 9. We see that variations in the methylation parameters ρ and K_2 affect the sensitivity of the period with respect to other parameters in the model and these changes are most dramatic as the sensitivities diverge in the neighborhood of the Hopf bifurcation. Since it would be risky for a biological clock to operate close to a Hopf bifurcation and the sensitivities are relatively unaffected by the methylation parameters away from the Hopf bifurcation, we see that the period is robust to changes in the methylation parameters. As in Fig. 8, where higher ρ values cause the bifurcation to occur for lower values of K_2 , Fig. 9 shows that higher values of ρ cause the sensitivity curves to diverge for lower K_2 . One could interpret this finding as saying that lower ρ values allow the model to tolerate more methylation (larger K_2 value) before becoming arrhythmic.

F. Transcription function in the no-methylation limit

In this section we explore the extent to which the influence of methylation in the reduced IT-MFL model can be reproduced in the no-methylation limit ($K_2 = 0 = \rho$). We investigate this by adjusting the transcription rate ρ_f of the inactive promoter state. To make this comparison, we altered our derivation of the reduced IT-MFL model to allow a nonzero value of ρ_f . This results in the transcription function

$$T(\tilde{B}_{\text{tot}}) = \left(\frac{\tilde{A}_{\text{qss}}(\tilde{B}_{\text{tot}})\tilde{K}_1}{1 + K_2 + \tilde{A}_{\text{qss}}(\tilde{B}_{\text{tot}})\tilde{K}_1} \right) \left(1 - \rho' - \frac{(\rho - \rho')K_2}{1 + K_2} \right) + \frac{(\rho - \rho')K_2}{1 + K_2} + \rho', \quad (50)$$

in which $\rho' = \rho_f / \rho_b$, and Eqs. (42) to (44) remain otherwise unchanged. We used numerical optimization to find

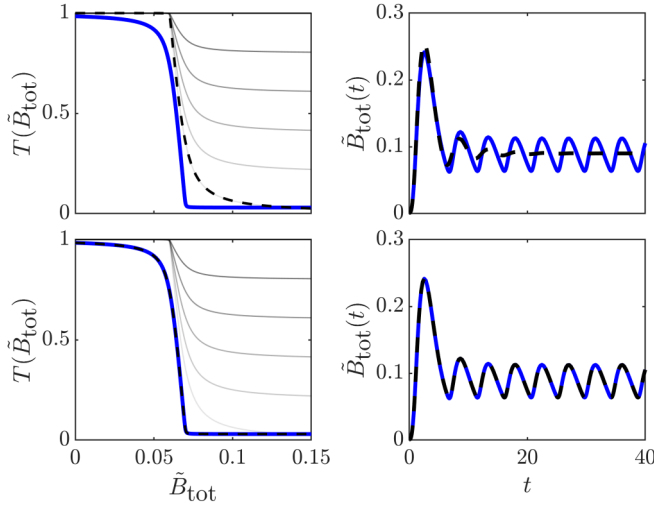


FIG. 10. Varying ρ' does not compensate for the effects of methylation, but it is possible to compensate for these effects by varying both ρ' and \tilde{K}_1 . (Top left) The transcription function of the reduced IT-MFL model with methylation is shown in blue, and the dashed black line shows the best approximation under the constraint that $K_2 = 0 = \rho$, $\rho' \in [0, 1]$, and all other parameters are fixed. Transcription functions with $\rho' \in [0, 1]$ and $K_2 = 0 = \rho$ are shown in gray, with darker lines representing higher levels of ρ' . (Top right) When only ρ' is allowed to vary, there is a qualitative difference between the dynamics produced by the methylated transcription function shown in blue, and those produced by the best approximation shown with the dashed black line. (Bottom left) By allowing both ρ' and \tilde{K}_1 to vary, we obtain a good approximation of the methylated transcription function (bottom right) and good agreement in their trajectories $\tilde{B}_{\text{tot}}(t)$. Fixed parameters: $\tilde{K}_d = 10^{-7}$, $\tilde{A}_{\text{tot}} = 7 \times 10^{-2}$, $\tilde{g}_{\text{tot}} = 10^{-2}$. In the methylated case, $\rho' = 0$, $\rho = 3 \times 10^{-2}$, $K_2 = 3 \times 10^2$ and in the unmethylated case $\rho = K_2 = 0$ and $\rho' \in [0, 1]$. In the top row $\tilde{K}_1 = 3 \times 10^5$ and in the bottom row \tilde{K}_1 was optimized over the interval $[10^{-5}, 10^7]$ and an optimal value of $\tilde{K}_1 \approx 10^3$ was found. Transcription functions were optimized in the L^∞ norm; similar results were obtained using the L^2 norm.

the best approximation of the transcription function in the no-methylation limit and then assessed the quality of the approximation by comparing the limit-cycle trajectory $\tilde{B}_{\text{tot}}(t)$. Since ρ_b is held constant and only the dimensionless ratio $\rho' = \rho_f/\rho_b$ affects the dynamics, we varied ρ' instead of ρ_f . Figure 10 confirms that the influence of methylation on the model cannot be reproduced by altering the value ρ' alone. By comparing a variety of methylation levels, we find this difference was most pronounced for high values of K_2 and low values of ρ . This is to be expected since K_2 must be large for methylation to have a nontrivial effect, and a higher value of ρ translates the transcription function upward, making it easier to approximate the function by simply increasing ρ' . A much better approximation can be found by varying \tilde{K}_1 and ρ' simultaneously, as shown in the bottom two panels of Fig. 10.

The results of Fig. 10 suggest that methylation allows the system to operate with an effectively lowered value of \tilde{K}_1 . In other words, methylation may be a mechanism for the clock to tune the value of \tilde{K}_1 which is crucial for generating the nonlinearity necessary for oscillatory behavior. Since the equilibrium constants \tilde{K}_1 and K_2 are regulated

by a variety of factors, some of which may be shared, it is difficult to argue that K_2 is more easily modified than \tilde{K}_1 in a real organism. At the same time, there is substantial experimental evidence that points to the integral role of methylation in the circadian clock [35]. Certainly our model is a vast simplification of this reality, however, it is positive to see that the influence of methylation in our model is more complex than a mere vertical translation of the transcription function.

IV. DISCUSSION

We introduced and analyzed a mathematical model of a mixed feedback loop with an intermediate promoter state. By extending the perturbative analysis of François and Hakim, we found that the uniqueness and stability of its equilibrium solution were preserved provided that the transcription rate of the new promoter state was between the inactive and active transcription rates. Under some additional restrictions on the parameters, we derived leading-order estimates for the period in the IT-MFL model as well as bounds for the difference in period between the MFL and IT-MFL models. Following our perturbative analysis, we used a different set of assumptions on the parameters to show how a modified Goodwin oscillator model, previously studied by Kim and Forger, can be obtained as an approximation of the IT-MFL model. Working in a generalization of this approximation, we found that, although methylation influences the period and its sensitivity to other parameters in the reduced IT-MFL model, excessive methylation can remove oscillations from the system. We also identified a parameter set where oscillations were lost upon the removal of methylation and could not be restored by varying ρ' alone. Since the assumptions for the reduced IT-MFL model are more general than those used in our derivation of the Kim-Forger model, we believe a systematic comparison of these two models viewed as approximations of the full IT-MFL model would be a valuable contribution to the literature.

Our perturbative analysis produced sufficient conditions, such as the requirement that $\rho_2 < \rho_1$, for controlling the IT-MFL model by the MFL model. For instance, the period estimates, monostability conditions, and linear stability of the IT-MFL model could all be phrased in terms of the corresponding behavior in the MFL model. In future work, one could test if inequalities of the form $\rho_i < \rho_1$ allow for similar estimates when one generalizes to an n -promoter state mixed feedback loop model. In addition, incorporating DNA methylation machineries, namely DNA methyltransferases (DNMTs) and Ten-eleven translocation enzymes (TETs), as well as cellular states that influence DNA modifications (e.g., development, aging, or even cancer) may provide a better representation of biological reality. These features may introduce sufficient nonlinearity for the model to stay rhythmic at higher methylation levels, allowing methylation to play a greater role in controlling the periodic behavior [36]. Although such a model would likely be too detailed for the type of analysis we used here, we hope our results will provide a useful starting point for analyzing such an extension. Future work will attempt to explore the role of oscillatory patterns in

DNA modifications seen in cell fate determination, aging, and disease [1,2].

Molecular noise is another biologically important factor [37,38] which could be studied in future work. The recent work of Karapetyan and Buchler on a stochastic generalization of the MFL model [25] and the work of Wang and Peskin on the effects of molecular noise on entrainment in an MFL model of the circadian clock [20] provide useful starting points for extending our analysis to the stochastic setting. More generally, several stochastic models of methylation [39–41] and histone [42–44] dynamics, as well as biophysical epigenetic models [45,46] have appeared in recent years. As it becomes more common practice to include epigenetic effects in gene regulatory network models, see, for example, [47–50], we anticipate the detailed stand-alone models of epigenetic dynamics will come to be useful in

gene regulatory network models. It has been argued that the incorporation of epigenetic factors in mathematical models of gene regulatory networks is one of the most important challenges in the development of large-scale predictive models of postembryonic systems [51]. As these models come into existence, we expect studies of reduced models will continue to provide unique insights into the intricate machinery of regulated gene expression, unavailable through detailed model simulation alone.

ACKNOWLEDGMENTS

We thank the reviewers for their insightful comments. A.R.S. acknowledges the support of the Natural Sciences and Engineering Research Council of Canada (NSERC): RGPIN-2019-06946.

- [1] E. S. Oh and A. Petronis, Origins of human disease: The chrono-epigenetic perspective, *Nat. Rev. Genet.* **22**, 533 (2021).
- [2] A. Parry, S. Rulands, and W. Reik, Active turnover of DNA methylation during cell fate decisions, *Nat. Rev. Genet.* **22**, 59 (2021).
- [3] S. Horvath and K. Raj, DNA methylation-based biomarkers and the epigenetic clock theory of ageing, *Nat. Rev. Genet.* **19**, 371 (2018).
- [4] G. Oh, S. Ebrahimi, M. Carlucci, A. Zhang, A. Nair, D. E. Groot, V. Labrie, P. Jia, E. S. Oh, R. H. Jeremian, M. Susic, T. C. Shrestha, M. R. Ralph, J. Gordevičius, K. Koncėvičius, and A. Petronis, Cytosine modifications exhibit circadian oscillations that are involved in epigenetic diversity and aging, *Nat. Commun.* **9**, 644 (2018).
- [5] G. Oh, K. Koncėvičius, S. Ebrahimi, M. Carlucci, D. E. Groot, A. Nair, A. Zhang, A. Kriščiūnas, E. S. Oh, V. Labrie *et al.*, Circadian oscillations of cytosine modification in humans contribute to epigenetic variability, aging, and complex disease, *Genome Biol.* **20**, 2 (2019).
- [6] S. Rulands, H. J. Lee, S. J. Clark, C. Angermueller, S. A. Smallwood, F. Krueger, H. Mohammed, W. Dean, J. Nichols, P. Rugg-Gunn *et al.*, Genome-scale oscillations in DNA methylation during exit from pluripotency, *Cell Syst.* **7**, 63 (2018).
- [7] S. Kangaspeska, B. Stride, R. Métivier, M. Polycarpou-Schwarz, D. Ibberson, R. P. Carmouche, V. Benes, F. Gannon, and G. Reid, Transient cyclical methylation of promoter DNA, *Nature (London)* **452**, 112 (2008).
- [8] R. Métivier, R. Gallais, C. Tiffocche, C. Le Péron, R. Z. Jurkowska, R. P. Carmouche, D. Ibberson, P. Barath, F. Demay, G. Reid *et al.*, Cyclical DNA methylation of a transcriptionally active promoter, *Nature (London)* **452**, 45 (2008).
- [9] A. Azzi, R. Dallmann, A. Casserly, H. Rehauer, A. Patrignani, B. Maier, A. Kramer, and S. A. Brown, Circadian behavior is light-reprogrammed by plastic DNA methylation, *Nat. Neurosci.* **17**, 377 (2014).
- [10] C. H. Ko and J. S. Takahashi, Molecular components of the mammalian circadian clock, *Hum. Mol. Genet.* **15**, R271 (2006).
- [11] P. François and V. Hakim, Design of genetic networks with specified functions by evolution in silico, *Proc. Natl. Acad. Sci. USA* **101**, 580 (2004).
- [12] B. C. Goodwin, Oscillatory behavior in enzymatic control processes, *Adv. Enzyme Regul.* **3**, 425 (1965).
- [13] P. François and V. Hakim, Core genetic module: The mixed feedback loop, *Phys. Rev. E* **72**, 031908 (2005).
- [14] P. François, A model for the neurospora circadian clock, *Biophys. J.* **88**, 2369 (2005).
- [15] R. L. Bar-Or, R. Maya, L. A. Segel, U. Alon, A. J. Levine, and M. Oren, Generation of oscillations by the p53-Mdm2 feedback loop: A theoretical and experimental study, *Proc. Natl. Acad. Sci. USA* **97**, 11250 (2000).
- [16] J. Monod and F. Jacob, General conclusions: Teleonomic mechanisms in cellular metabolism, growth, and differentiation, in *Cold Spring Harbor Symposia on Quantitative Biology* (Cold Spring Harbor Laboratory Press, Cold Spring Harbor, NY, 1961), Vol. 26, pp. 389–401.
- [17] J. K. Kim and D. B. Forger, A mechanism for robust circadian timekeeping via stoichiometric balance, *Mol. Syst. Biol.* **8**, 630 (2012).
- [18] J. K. Kim, Z. P. Kilpatrick, M. R. Bennett, and K. Josić, Molecular mechanisms that regulate the coupled period of the mammalian circadian clock, *Biophys. J.* **106**, 2071 (2014).
- [19] J. K. Kim, Protein sequestration versus Hill-type repression in circadian clock models, *IET Syst. Biol.* **10**, 125 (2016).
- [20] G. Wang and C. S. Peskin, Entrainment of a cellular circadian oscillator by light in the presence of molecular noise, *Phys. Rev. E* **97**, 062416 (2018).
- [21] D. DeWoskin, W. Geng, A. R. Stinchcombe, and D. B. Forger, It is not the parts, but how they interact that determines the behaviour of circadian rhythms across scales and organisms, *Interface Focus* **4**, 20130076 (2014).
- [22] N. E. Buchler and M. Louis, Molecular titration and ultrasensitivity in regulatory networks, *J. Mol. Biol.* **384**, 1106 (2008).
- [23] N. E. Buchler and F. R. Cross, Protein sequestration generates a flexible ultrasensitive response in a genetic network, *Mol. Syst. Biol.* **5**, 272 (2009).
- [24] B. P. Ingalls, *Mathematical Modeling in Systems Biology: An Introduction* (MIT Press, Cambridge, MA, 2013).
- [25] S. Karapetyan and N. E. Buchler, Role of DNA binding sites and slow unbinding kinetics in titration-based oscillators, *Phys. Rev. E* **92**, 062712 (2015).

- [26] B. Nagy, Bifurcations of a one-loop circadian rhythm model, *Internat. J. Qual. Theory Differ. Equ.* **4**, 2 (2018).
- [27] P. L. Simon, H. Farkas, and M. Wittmann, Constructing global bifurcation diagrams by the parametric representation method, *J. Comput. Appl. Math.* **108**, 157 (1999).
- [28] C. M. Bender and S. A. Orszag, *Advanced Mathematical Methods for Scientists and Engineers I: Asymptotic Methods and Perturbation Theory* (Springer Science & Business Media, New York, 2013).
- [29] See Supplemental Material at <http://link.aps.org/supplemental/10.1103/PhysRevE.105.034411> for more information on the promoter methylation in a mixed feedback loop circadian clock model.
- [30] D. B. Forger, Signal processing in cellular clocks, *Proc. Natl. Acad. Sci. USA* **108**, 4281 (2011).
- [31] J. Mallet-Paret and H. L. Smith, The Poincaré-Bendixson theorem for monotone cyclic feedback systems, *J. Dyn. Differ. Equ.* **2**, 367 (1990).
- [32] E. L. Allgower and K. Georg, *Introduction to Numerical Continuation Methods* (SIAM, Philadelphia, 2003).
- [33] Y. A. Kuznetsov, *Elements of Applied Bifurcation Theory*, Vol. 112 (Springer Science & Business Media, New York, 2013).
- [34] B. P. Ingalls, Autonomously oscillating biochemical systems: Parametric sensitivity of extrema and period, *Syst. Biol.* **1**, 62 (2004).
- [35] J.-M. Fustin, S. Ye, C. Rakers, K. Kaneko, K. Fukumoto, M. Yamano, M. Versteven, E. Grünewald, S. J. Cargill, T. K. Tamai *et al.*, Methylation deficiency disrupts biological rhythms from bacteria to humans, *Commun. Biol.* **3**, 211 (2020).
- [36] M. V. Greenberg and D. Bourçhis, The diverse roles of DNA methylation in mammalian development and disease, *Nat. Rev. Mol. Cell Biol.* **20**, 590 (2019).
- [37] A. Raj and A. van Oudenaarden, Nature, nurture, or chance: Stochastic gene expression and its consequences, *Cell* **135**, 216 (2008).
- [38] A. R. Stinchcombe, C. S. Peskin, and D. Tranchina, Population density approach for discrete mRNA distributions in generalized switching models for stochastic gene expression, *Phys. Rev. E* **85**, 061919 (2012).
- [39] K. Utsey and J. P. Keener, A mathematical model for inheritance of DNA methylation patterns in somatic cells, *Bull. Math. Biol.* **82**, 84 (2020).
- [40] M. Ancona, D. Michieletto, and D. Marenduzzo, Competition between local erasure and long-range spreading of a single biochemical mark leads to epigenetic bistability, *Phys. Rev. E* **101**, 042408 (2020).
- [41] L. Busto-Moner, J. Morival, H. Ren, A. Fahim, Z. Reitz, T. L. Downing, and E. L. Read, Stochastic modeling reveals kinetic heterogeneity in post-replication DNA methylation, *PLoS Comput. Biol.* **16**, e1007195 (2020).
- [42] A. Sood and B. Zhang, Quantifying epigenetic stability with minimum action paths, *Phys. Rev. E* **101**, 062409 (2020).
- [43] A. Sood and B. Zhang, Quantifying the stability of coupled genetic and epigenetic switches with variational methods, *Front. Genet.* **11**, 1837 (2021).
- [44] B. Bhattacharyya, J. Wang, and M. Sasai, Stochastic epigenetic dynamics of gene switching, *Phys. Rev. E* **102**, 042408 (2020).
- [45] D. Jost, Bifurcation in epigenetics: Implications in development, proliferation, and diseases, *Phys. Rev. E* **89**, 010701(R) (2014).
- [46] R. Cortini, M. Barbi, B. R. Caré, C. Lavelle, A. Lesne, J. Mozziconacci, and J. M. Victor, The physics of epigenetics, *Rev. Mod. Phys.* **88**, 025002 (2016).
- [47] T. Chen, M. A. Al-Radhawi, and E. D. Sontag, A mathematical model exhibiting the effect of DNA methylation on the stability boundary in cell-fate networks, *Epigenetics* **16**, 436 (2021).
- [48] W. Jia, A. Deshmukh, S. A. Mani, M. K. Jolly, and H. Levine, A possible role for epigenetic feedback regulation in the dynamics of the epithelial–mesenchymal transition (EMT), *Phys. Biol.* **16**, 066004 (2019).
- [49] M. Flöttmann, T. Scharp, and E. Klipp, A stochastic model of epigenetic dynamics in somatic cell reprogramming, *Front. Physiol.* **3**, 216 (2012).
- [50] N. Folguera-Blasco, R. Pérez-Carrasco, E. Cuyàs, J. A. Menendez, and T. Alarcón, A multiscale model of epigenetic heterogeneity-driven cell fate decision-making, *PLoS Comput. Biol.* **15**, e1006592 (2019).
- [51] E. V. Rothenberg, Causal gene regulatory network modeling and genomics: Second-generation challenges, *J. Comput. Biol.* **26**, 703 (2019).